AGU PUBLICATIONS

Water Resources Research

RESEARCH ARTICLE
10.1002/2015WR017116

Key Points:
- Stony debris flow dynamics in confluence setting
- Slope angle and triggering scenario control, respectively, mobility and morphology
- Main channel morphology at confluences

Correspondence to:
L. M. Stancanelli,
lmstanca@dica.unict.it

Citation:
Stancanelli, L. M., S. Lanzoni, and E. Foti (2015), Propagation and deposition of stony debris flows at channel confluences, *Water Resour. Res.*, *51*, 5100–5116, doi:10.1002/2015WR017116.

Received 24 FEB 2015
Accepted 3 JUN 2015
Accepted article online 6 JUN 2015
Published online 4 JUL 2015

Propagation and deposition of stony debris flows at channel confluences

L. M. Stancanelli[1], S. Lanzoni[2], and E. Foti[1]

[1]Department of Civil Engineering and Architecture, University of Catania, Catania, Italy, [2]Department of Civil, Architectural and Environmental Engineering, University of Padua, Padua, Italy

Abstract The fluid dynamics of stony debris flows generated in two small tributaries adjacent to each other and flowing into a main receiving channel was analyzed experimentally at a laboratory scale. The analysis on the propagation along the tributaries and deposition in the main channel provide information about sediment-water mobility, dangerous damming, and potential hazard. Debris flows were generated by releasing a preset water discharge over an erodible layer of saturated gravels material. As a consequence, the debris flow sediment concentration varied accordingly to the entrainment rate which, in turn, was strongly controlled by the tributary slope. The data collected by acoustic level sensors, pore fluid pressure transducers, and a load cell were used to characterize the evolution of bulk density and solid concentration of the sediment-water mixture. These two parameters were relevant to assess the stony debris flow mobility which contributes to determine the shape of sediment deposits in the main channel. The detailed bed topography surveys carried out in the main channel at the end of each experiment provided information on the morphology of these deposits and on the interplay of adjacent confluences. The influences of confluence angle, tributary slopes, and triggering conditions have been investigated, for a total of 18 different configurations. Within the investigated range of parameters, the slope angle was the parameter that mainly influences the stony debris flow mobility while, for adjacent confluences, the degree of obstruction within the receiving channel was strongly influenced by the triggering scenario.

1. Introduction

Debris flows generally form in narrow steep valleys when loose masses of unconsolidated debris become unstable under the action of water supplied by rainfalls or snow melting [e.g., *Sharp and Nobles*, 1953; *Sitar et al.*, 1992]. The water-sediment mixture triggered by the water flow then propagates downstream, possibly entraining further sediment and water from the bed or the banks [*Iverson*, 2013].

We focused our attention on sediment mobility along scree slopes and steep mountain torrents associated with a particular type of debris flows, classified as stony by *Takahashi* [2007], consisting of relatively coarse grains and a low content of fine particles [*Bonnet-Staub*, 1999]. In particular, we investigated experimentally how the mobilized sediment subsequently deposits at two consecutive confluences, tending to obstruct the receiving channel.

Stony debris flows are common in mountain torrents of Austrian, Italian, and Swiss Alps [*Scheidl and Rickenmann*, 2009] and in gravel bedded channels originating in the scree slopes located at the base of rock faces (e.g., in the Dolomites, Northern Italy) [*Gregoretti and Dalla Fontana*, 2008]. They are usually triggered by surface runoff following intense rainfall events. Hydrodynamic forces destabilize the gravel bed surface, determining the dispersion of sediment grains throughout the entire flow depth [*Lanzoni and Tubino*, 1993; *Tognacca et al.*, 2000; *Gregoretti*, 2000]. Due to their inertia, the large masses of mobilized sediment can travel for long distances and eventually deposit where friction actions prevail, namely for low enough hillslopes, or when discharging in broad alluvial fans and in a less steep channel.

In stony debris flows the distribution of particle sizes consists mainly of boulders, cobbles, and gravel [*Bonnet-Staub*, 1999; *Takahashi*, 2007]. Finer fractions (less than 1 mm) are likely contained in the interstitial muddy water which behaves as a liquid. In any case, fraction of constituent less than 0.1 mm is far less than in viscous-type and muddy-type debris flows [*Takahashi*, 2007]. The dynamics of stony-type flows is thus dominated by grain collision stresses which are responsible of the dispersion of grains throughout the

entire flow depth (mature flow) and segregation processes (e.g., the accumulation of larger particles on the debris front). The excess of pressure in the pore fluid is likely to play a minor role especially for low grain concentrations, because of large voids between particles [*Takahashi*, 2007].

In the present contribution we have considered with particular attention the dynamics of multiple debris flow tributaries that join a main river reach. Such a dynamics, which is rather frequent in the Dolomites (Northern Italy) [*Gregoretti and Dalla Fontana*, 2008], can have dramatic effects in terms of loss of human lives and damages. The debris depositing in the recipient channel, in fact, may create a significant degree of obstruction or even a debris dam, depending on the amount of mobilized sediment and the momentum ratio between the tributary and the mainstream [*Dang et al*., 2009]. In any case, the localized input of coarse sediment at a confluence introduces a perturbation of the sediment composition in the main channel which could affect its longitudinal morphology [*Sklar et al*., 2006].

Owing to the complexity of the interactions between the incoming solid-liquid mixture conveyed by the debris flow and the receiving water current, attempts to tackle the problem numerically are still in an early stage [*Chen et al*., 2011; *Chen and Peng*, 2006; *Chen et al*., 2013]. Debris flow and water flow are simulated independently, and the interaction between the two types of flows is accounted for in a simplified manner [*Chen et al*., 2011, 2013]. The geometry of deposition fans has then been studied experimentally, with particular attention to the case of a single confluence. The experiments carried out by suddenly releasing in a flume a given volume of water and sediment mixed together [*Chen et al*., 2004; *Chen and An*, 2007] suggest that the main factors influencing the fan geometry are the confluence angle, the tributary slope, the sediment concentration of the incoming debris flow and the liquid discharge along the receiving channel. Three different types of blockage (complete blockage, or semiblockage spanning either partially or completely the channel width) were observed experimentally by *Dang et al*. [2009], depending on the momentum ratio between the tributary and the mainstream and the particle size distribution of the debris flow.

To authors' knowledge, no experiments addressing the morphology of sediment deposits that form in a main channel as a consequence of the material delivered by neighboring debris flows are available in the literature. The aim of the present contribution is to understand the dynamics of this type of confluence settings in the case of stony debris flows. In particular, we investigated experimentally how the mobilized sediment subsequently deposits at two consecutive confluences, tending to obstruct the receiving channel. Overland flow over a loose sediment bed, rather than an impulsive release of a premixed volume of water and sediment, was used to generate the debris flow. The mixture concentration was thus determined by the flume slope. The variables investigated in order to synthesize debris flow dynamics were the flow thickness, the bulk density of the sediment-water mixture, the sediment concentration, the total normal stress, and the pore fluid pressure. The geometry of sediment deposits in the receiving channel has been analyzed on the basis of tributary slope, confluence angle, and the possible triggering sequences which characterize multiple confluences. Finally, in order to identify the most dangerous configuration in terms of shrinkage of the hydraulic section, we determined the location of the center of mass, the volume, and the shape of the sediment deposits surveyed along the main channel at the end of each experiment.

2. Material and Methods

2.1. Experimental Apparatus

The experimental apparatus (Figure 1) consisted of two tributary flumes (B, upstream; C, downstream) 3 m long, 0.3 m wide, and 0.3 m deep, connected to a main channel (A) of length 10 m, width 0.5 m, and depth 0.7 m. The tributary flumes were located on the left side of the main channel, at an interaxis of 2.7 m. The junction between each tributary flume and the main channel was made through a particular joint system which allowed variations of both tributary slope and confluence angle. An U-shaped metal sheet, suitably designed for each confluence angle, ensured a smooth connection between the main channel and the tributary section. A PVC layer enveloped the entire junction to avoid water losses. The lateral walls of the main channel and of the tributary flumes were made by glass and Plexiglas, respectively. The fixed bed surface of all flumes was roughened by gluing a layer of the sediment used in the experiments. These sediment consisted of nearly uniform gravel with mean particle diameter $d_s = 3$ mm, density $\rho_s = 2650$ kg/m^3, closest packing sediment concentration $c^* = 0.62$, dry and submerged angles of repose $\varphi = 48.6°$ and $\varphi_s = 43.3°$. This type of sediment, without any content of fine fractions, has been chosen consistently with the small

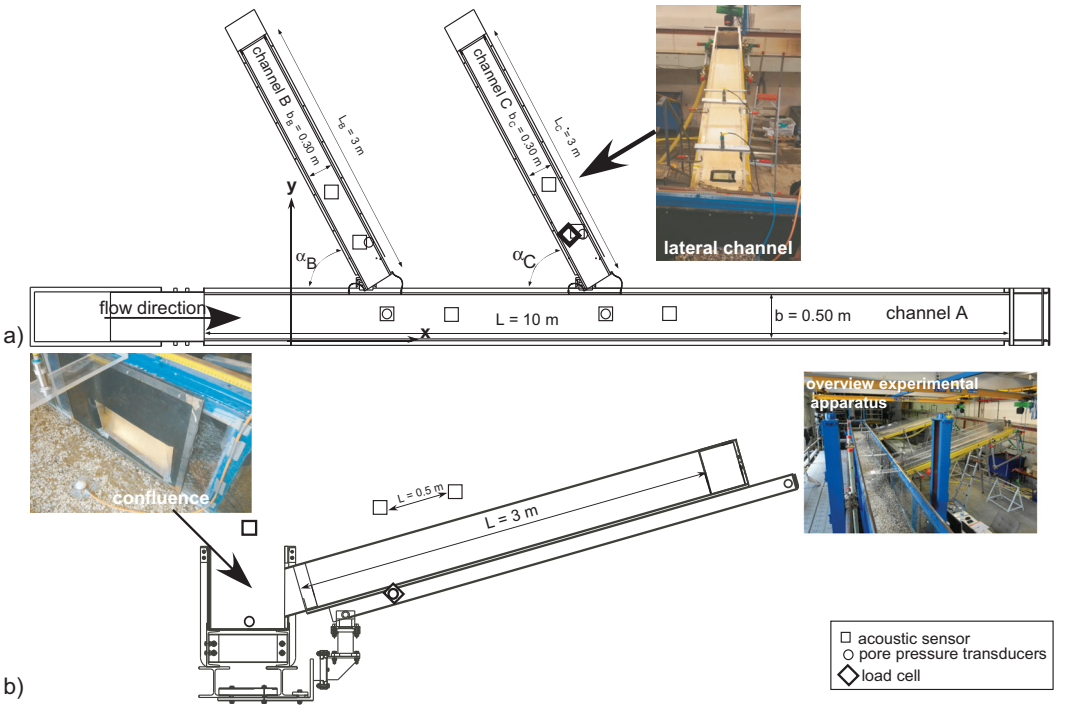

Figure 1. Overall sketch of the experimental apparatus and locations of the various measuring devices. (a) Plan view of the main channel (A) and of the two tributary flumes (B, upstream, and C, downstream). (b) Lateral view of the downstream tributary flume and of its confluence with the main channel.

amounts of fines (content of particles less than 1 mm smaller than about 20%), as well as the relatively low values of the bulk concentration (roughly in the range 0.35–0.6) typical of stony debris flows [*Bonnet-Staub*, 1999; *Takahashi*, 2007]. The possible effects of finer sediment fractions are discussed section 4.

Various instruments have been used for investigating the propagation and deposition of the sediment-water mixtures generated in the tributaries. The lateral flume C was equipped with a load cell (54-5-C3 Celmi, application range of 0–5 kg, error 0.02%FS), a pore pressure transducer (PR 9L keller, working range 0–0.1 bar, error 0.1%FS), and an acoustic level sensor (Pepperl + Fuchs, application range 0–0.5 m, error 0.001 m) to measure the time distributions of total normal stress, interstitial fluid pressure, and surface elevation of the sediment-water mixture triggered in the flume. These instruments were placed 0.5 m from the downstream end section of the flume. The load cell and the pressure transducer were located on the rigid bed of the flume. In particular, the latter was accommodated in a cavity of the bed, filled with water and covered at the top with a thin steel grid in order to separate water from sediment. A video camera, filming the lateral side of the flume, was used to identify the thickness of the moving sediment-water mixture. Other seven acoustic level sensors (Pepperl + Fuchs) were located along the various flumes (see Figure 1) to monitor the flow level during the propagation and deposition of the debris flow.

2.2. Experiments

The experiments consisted in triggering stony debris flows in two different tributary channels and letting them to merge into a main, less sloping channel, where sediments eventually deposited, under the reworking action of a preset water discharge. The relevant parameters varied in the tests to investigate the degree of blockage in the main channel were: the tributary slope, the confluence angle, and triggering sequence.

At the beginning of each test, the main channel was tilted at a slope of 5° and a water flow rate $Q_A = 5$ l/s was discharged along it (flow depth 8 mm), flowing over its rough fixed bed. The two tributary flumes were arranged with the same slopes and confluence angles. Each of them was filled with a layer of loose sediment of thickness about 9 cm, covering completely the rough fixed bed. This static sediment bed was suitably flattened and preliminary saturated. Seepage flow was made possible by a permeable sill located at

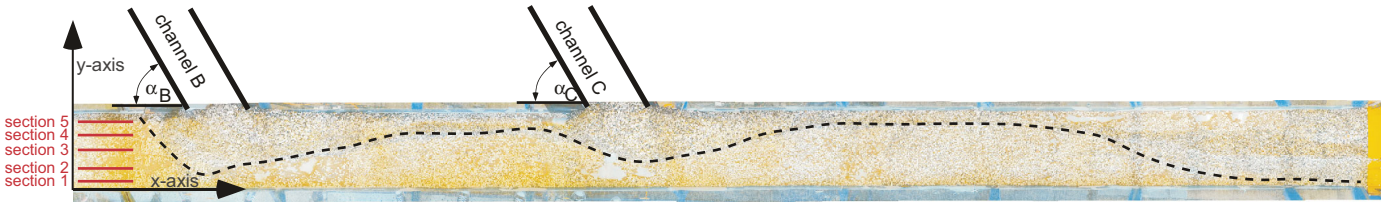

Figure 2. Top view of the material deposited along the main channel (A) at the end of test 1 (tributary slope 17°; confluence angle 60°; downstream triggering sequence). The dashed line pinpoints the deposit contour, while the straight segments on the left side localize the longitudinal section along which the bed topography has been measured.

the end of the flume which sustained the loose sediment bed despite the slope, while allowing groundwater flow. Debris flows were subsequently triggered by releasing abruptly a prescribed water discharge (Q_B or Q_C) from the tank located at the head of each tributary channel. Release times (t_B and t_C) depended on the considered triggering scenarios, the possible difference in triggering times being about 3 min.

As documented by video camera records, the water flowing over the loose sediment bed initially placed in the tributaries caused the erosion and entrainment of grains in the upstream reach of the flume, until enough material was provided for the formation of the debris flow front. This front then propagated downstream with almost negligible erosion of the underlying static sediment layer. Contemporaneously, the debris flow body elongated owing to the entrainment of the material in the tail. Given the relatively high tributary flume slopes considered in the experiments, mature debris flow conditions (with sediment grains dispersed throughout the entire flow depth) were established quite rapidly in all the tests [*Lanzoni and Tubino*, 1993; *Takahashi*, 2007].

After the debris flows propagated along a tributary channel, the mobilized material flowed into the main channel and eventually deposited within it. Each experiment was stopped when morphological changes of the sediment deposits, caused by the water flowing in the main channel, were negligibly small. The duration of a given experiment depended on the tributary slope (longer times being associated with smaller slopes). The data collected during a given experiment consisted of temporal records of debris flow surface elevation, H, measured through the acoustic level sensor; elevation of the interface with the static sediment bed, H_{sb}, determined through analysis of video records; total normal stress, σ_{fb}, and pore fluid pressure p_{fb}, both measured in the fixed bed of the tributary flume, 0.5 m ($\sim$ 1.7 times the flume width) from the end section (see Figure 1). The deposit morphology at the end of each run was analyzed on the basis of five longitudinal bed sections (see Figure 2) surveyed in the main channel (2 cm apart) through a point gauge.

The quantities varied in the present series of tests (18) are summarized in Table 1. They are the tributary slope β (15° and 17°), the confluence angle α (90°-60°-50°), and the triggering scenarios (debris flows occurring simultaneously in the tributaries ($t_B = t_C$), or occurring first either in the upstream ($t_B < t_C$) or in the downstream ($t_B > t_C$) tributary).

Possible effects of the main channel discharge in shaping the final sediment deposits are discussed in section 4. The seepage discharge needed to saturate the static sediment bed initially placed in each tributary depended on the slope adopted in the test and varied between 0.7 and 0.8 l/s. The triggering discharge varied in the range 2.7–3.4 l/s and determined the destabilization of the initial bed and the consequent formation of the debris flow. The range of confluence angles investigated has been selected on the basis of the configurations typically observed in the field [*Benda*, 1990; *Millard*, 1999; *Miller and Burnett*, 2008]. The choice of tributary slopes was made after a preliminary set of tests (not reported in Table 1) aiming to determine the conditions needed to generate mature stony debris flows [*Takahashi*, 1991; *Lanzoni and Tubino*, 1993], with sediment grains dispersed across the entire flow depth. Smaller slopes imply the formation of immature debris flows, with a sediment-water mixture flowing beneath a distinct layer of clear water. On the other hand, too high slopes give rise to debris flows consisting of an unsteady front which progressively increases its thickness during the propagation, owing to the continuous entrainment of grains from the erodible bed.

2.3. Data Treatment

In the case of a stony debris flow generated by a given water discharge (Q) flowing over a layer of erodible material (of thickness H_0), the dynamics of the phenomenon can be described in terms of the basal normal

Table 1. Summary of the Relevant Parameters Characterizing the Present Tests[a]

	Main Channel (A)		Upstream Tributary (B)				Downstream Tributary (C)			
Test	β (°)	Q (l/s)	β (°)	α (°)	t (s)	Q (l/s)	β (°)	α (°)	t (s)	Q (l/s)
1	5	5.0	17	60	0	3.4	17	60	168	3.2
2	5	5.2	17	60	176	3.4	17	60	0	3.2
3	5	5.0	17	60	0	3.4	17	60	0	3.2
4	5	5.2	17	50	0	3.4	17	50	175	3.2
5	5	5.1	17	50	222	3.4	17	50	0	3.2
6	5	5.1	17	50	0	3.4	17	50	0	3.2
7	5	5.0	15	50	0	3.4	15	50	210	3.2
8	5	5.0	15	50	227	3.4	15	50	0	3.2
9	5	5.1	15	60	0	2.8	15	60	0	2.8
10	5	5.1	15	60	0	2.8	15	60	214	2.7
11	5	5.0	15	60	219	2.8	15	60	0	2.7
12	5	5.0	15	50	0	2.8	15	50	0	3.0
13	5	5.1	15	90	0	2.7	15	90	0	2.9
14	5	5.1	17	90	0	2.8	17	90	0	2.8
15	5	5.1	17	90	0	3.1	17	90	235	2.9
16	5	5.1	17	90	158	3.1	17	90	0	2.9
17	5	5.0	15	90	0	3.1	15	90	203	3.0
18	5	4.8	15	90	204	3.0	15	90	0	2.9

[a]The various quantities are defined as follows: β, slope angle; α, confluence angle; Q, triggering discharge; t, time at which a debris flow is triggered in a given tributary channel.

stress, σ_b, and pore fluid pressure, p_b, at the interface between the debris flow and the underlying static bed. These quantities are here obtained by decreasing the values measured at the rigid bed of the flume (i.e., σ_{fb} and p_{fb}) by the weight of the static layer ($\rho_{max}\, g\, (H-D)cos\beta$), and of the corresponding interstitial pore pressure, assumed to be distributed hydrostatically ($\rho_f\, g\, Hcos\beta$). Here D is the debris flow depth, determined as the difference $H-H_{sb}$ between the free surface elevation, H, and the elevation of the interface with the static sediment bed, H_{sb}. Moreover, ρ_{max} ($=\rho_s c_* + \rho_f(1-c_*)$) is the density of the static layer initially placed in the flume, assumed to be saturated and with a sediment volume concentration equal to its closest packing value.

In general, the assumption of hydrostatic fluid pore pressure implies that the relative motion between the solid and fluid phases is negligible. Denoting by κ the hydraulic permeability of the granular matrix, significant excess pore pressure gradients ($\sim g\,\rho_f \sim 10^4$ Pa/m) are expected to occur when the volumetric flux of pore fluid per unit area of mixture (specific discharge) exceeds 10^{-2} m/s for high values of the ratio κ/μ_f, and 10^{-10} m/s for debris flow with the smallest κ/μ_f [*Iverson*, 2013]. In the case treated here, intended to reproduce stony debris flow conditions, the relevant value of the hydraulic permeability ($k \sim 10^{-3}$ m/s) and the absence of fine particles in the pore fluid ($\mu_f \sim 0.001$ Pa/s) imply a relatively large ratio κ/μ_f and, hence, a rapid dissipation, through diffusion, of excess pore fluid pressure. The pore pressure can then be taken to be hydrostatically distributed along the direction normal to the flow, as it will be shown in section 3.1.

Further quantities estimated from the measurements are the bulk density ρ and sediment concentration C. Under the assumption that, as a first approximation, the local value of the sediment concentration keeps almost constant within the flow depth, we can write:

$$\rho = \frac{\sigma_b}{g\, D \cos\beta}, \tag{1}$$

while the relation between ρ and C reads:

$$\rho = \rho_s C + \rho_f (1-C). \tag{2}$$

2.4. Scaling Issues

Detailed field observations about debris flow mechanics are generally difficult to obtain [*Kailey et al.*, 2011]. Indeed, even if one is able to observe a real debris flow event, it may be difficult or even impossible to determine the boundary conditions and the key parameters influencing the flow behavior in the field. Hence, the contribution to the knowledge that physical models can provide is still precious. Both large and small-scale physical models have been widely used to investigate specific aspects of debris flow mechanics.

Denlinger and Iverson [2001] raised some concern about the uncertainties in the transfer of small-scale findings to real debris flows. On the other hand, the huge amount of material needed by large-scale experiments makes the design of the experimental apparatus and of the measurement setup cost intensive. For these reasons, experiments at the laboratory scale are still widely adopted. In addition, their capability of reducing the overall complexity of the phenomena allows to focus on the most relevant aspects of the mechanisms under investigation. In the present experimental campaign, the model-prototype similarity has been studied by applying the *calibration method* [see e.g., *Heller*, 2011]. Dimensionless parameters estimated for real-world prototypes are compared with those resulting from the physical model. If similar values are attained, provided that significant model and measurement effects can be ruled out, model-prototype similarity is reached. Observed model-prototype deviations may help to quantify-scale effects and their influence (through over or under-estimation) on the results. In particular, the following dimensional quantities have been considered: typical flow depth D, density ρ_s, volume concentration c_s, and mean diameter d_s of the sediment, density ρ_f and viscosity μ_f of the pore fluid, and typical shear rate $\dot{\gamma}$ of the flow.

In order to relate model observations to field conditions, the relative importance of inertial, viscous, and frictional forces in the experiments must match in the model and in the prototype [*Iverson*, 1997; *Hsu et al*., 2008]. Inertial forces arise from short-term collisions between sediment grains, viscous forces are controlled by pore fluid viscosity, and frictional forces are associated to long lasting contacts between grains. Their relative importance is described by three dimensionless numbers, N_{Bag}, N_{Sav}, and N_{mass}, which have been evaluated in the present experiments and compared with the values estimated in the field for various debris flow events.

The Bagnold number, N_{Bag}, measures the ratio of inertial to viscous stresses, and takes the form [*Iverson and Denlinger*, 2001]:

$$N_{Bag} = \frac{\rho_s \dot{\gamma} d_s^2 \lambda^{1/2}}{\mu_f}, \tag{3}$$

where the linear concentration λ is related to c_s and to the maximum possible grain concentration c_* through the relation $\lambda = c_s^{1/3}/(c_*^{1/3} - c_s^{1/3})$. The shear rate $\dot{\gamma}$ is computed in terms of the bulk flow characteristics as U/D, with U the surface flow speed.

The Savage number, N_{Sav}, defines the ratio of inertial to gravitational (and, hence, frictional) stresses, and can be written as [*Iverson and Denlinger*, 2001]:

$$N_{Sav} = \frac{\rho_s \dot{\gamma}^2 d_s^2}{(\rho_s - \rho_f) g D}, \tag{4}$$

where g is the magnitude of the gravitational acceleration.

Finally, the mass number, N_{mass}, expresses the importance of solid grain inertia to fluid inertia [*Iverson and Vallance*, 2001]:

$$N_{mass} = \frac{\rho_s c_s}{\rho_f (1 - c_s)}. \tag{5}$$

A sediment-water mixture flow tends to be dominated by grain collisions (inertial regime) when $N_{Sav} > 0.1$. Conversely, friction associated with persistent grain contacts (frictional regime) prevails for $N_{Sav} < 0.1$ [*Iverson and Denlinger*, 2001]. A collisional regime, whereby the bulk normal and shear stresses are proportional to $\dot{\gamma}^2$, is expected when $N_{Bag} > 450$, while macroviscous conditions, entailing a linear proportionality with $\dot{\gamma}$, are likely to occur for $N_{Bag} < 40$. Lastly, momentum transport by solid grain tends to prevail when $N_{mass} > 1$. Table 2 shows the values of the relevant dimensional quantities, of the corresponding dimensionless groups resulting from the present experiments, and those reported by *Iverson and Vallance* [2001] and *Hsu et al*. [2008] for either well documented field events or other laboratory experiments. The computations have been done by assuming that the volumetric sediment concentration c_s is approximately constant within the flow depth and, hence, equal to the bulk concentration C. The value of N_{mass} ($\sim$2) characterizing the present experiments is comparable with that observed in other experimental devices or estimated from field studies. The value of N_{Bag} ($\sim$1136), being much larger than 450, indicates a prevailing collision-dominated

Table 2. Values of Relevant Dimensional and Dimensionless Parameters Estimated for the Present Laboratory Experiments and Some Well-Documented Sediment-Water Flows[a]

	Present Tests	Drum Experiment Wet[b]	Small-Scale Flume[c]	USGS Flume[d]	Conveyor Belt Flume[e]	Kamikami-horizawa Debris Flow[f]	Mount St. Helens[g]	Elm Rock Avalanche[h]	Yake Dake Debris Flow[f]	Acquabona Debris Flow[i]
D (m)	0.05	0.05	0.04	0.2	0.04	2	1	5	2	2
ρ_s (kg/m^3)	2650	2650	2700	2700	1400	2700	2600	2400	2600	2650
ρ_f (kg/m^3)	1000	1000	1000	1000	1000	1000	2	2	1200	1200
c_s	0.43	0.55	0.5	0.6	0.6	0.6	0.3	0.5	0.6	0.6
d_s (m)	0.003	0.01	0.006	0.01	0.004	0.2	0.02	0.5	0.2	0.2
$\dot{\gamma}$ (s^{-1})	20	10	30	50	11	3	10	5	3	4
μ_f (Pas)	0.001	0.001	0.001	0.01	0.001	0.1	0.00002	0.00002	0.1	0.1
N_{mass}	2	3	3	4	2	4	557	1200	3	3
N_{Sav}	0.012	0.033	0.133	0.202	0.017	0.029	0.004	0.128	0.034	0.060
N_{Bag}	1136	9159	8307	588	1073	14110	910248	435397699	13588	18465

[a]To estimate Bagnold numbers, the maximum volume concentration of solid grains was set equal to 0.7 [*Iverson and Denlinger*, 2001].
[b]*Hsu et al.* [2008].
[c]*Iverson and Vallance* [2001].
[d]*Iverson* [1997].
[e]*Davies* [1990].
[f]*Takahashi* [1991].
[g]*Wilson and Head* [1981], *Kuntz et al.* [1981], and *Hoblitt* [1986].
[h]*Hsu* [1975, 1978].
[i]*Berti et al.* [1999, 2000].

regime, as typically occurs in mature stony debris flows. Further confirmation of the mature and stony character of present debris flows is provided by *Takahashi* [2007]: the small value (∼16) attained by the relative depth D/d_s (lower than 20–30); the values attained by the bulk solid concentration (larger than 0.2 and smaller than 0.5) and by the hydrostatic pore pressure distribution which, with good approximation, establishes within the flow depth (see results in section 3.1). The value attained by N_{Sav} (∼0.012) is of the same order of magnitude of those estimated by *Takahashi* [1991] for real stony debris flows. However, the fact that N_{Sav} is smaller than 0.1 suggests that frictional actions have a certain importance in determining the rheological behavior of the sediment-water mixture, as it will be discussed in section 4.

3. Analysis of Results

3.1. Propagation Phase

The data acquired by means of the pressure transducer, the load cell, and the acoustic sensor placed in the downstream tributary flume, combined with the video records taken at the transparent flume wall, provided the opportunity to identify the different phases which characterized the water-sediment mixture flow.

During each experiment the following phases clearly appeared: (i) initially dry and static sediment bed; (ii) saturation of the bed; (iii) passage of the front and body of the debris flow, with negligible erosion of the initial sediment bed; (iv) progressive erosion of the sediment bed owing to the passage of the debris flow tail. Figure 3 shows the time series of (a) total bed normal stress, σ_{fb}, and pore fluid pressure, p_{fb}, measured at the rigid bed of the flume; (b) elevations of the sediment-water mixture surface, H, and of the static sediment bed, H_{sb} recorded during run 14. At the beginning of the experiment ($t < 130$ s) all the monitored quantities are constant, owing to the static and dry condition of the loose sediment bed initially placed within the tributary channel. The saturation of this bed, starting at $t = 130$ s and ending a few seconds before the triggering of the debris flow, is characterized by the progressive adjustment of both the pore fluid pressure and the total load, while the surface elevation of the static bed does not vary. Note that the nonmonotonic behavior of the total bed stress ($130\ \text{s} < t \lesssim 300$ s) is related to a progressive adaptation to the groundwater flow of the solid matrix which, owing to the high slope, would tend to slide downstream as the seepage flow establishes, but is restrained by the porous bed sill located at the end of the flume. Debris flow is triggered in the upstream portion of the tributary at $t = 324$ s by overland flow. A sediment-water mixture forms and propagates downstream until the front reaches the monitored section ($t = 328$ s). The passage of the body is observed in the interval $t = 329$–337 s, with a minor erosion of the underlying static sediment bed. Finally, the sediment bed is progressively eroded during the passage of the tail ($t > 343$ s) and is totally washed out for $t = 355$ s. The debris flow propagation (lasting about 23 s) is similar

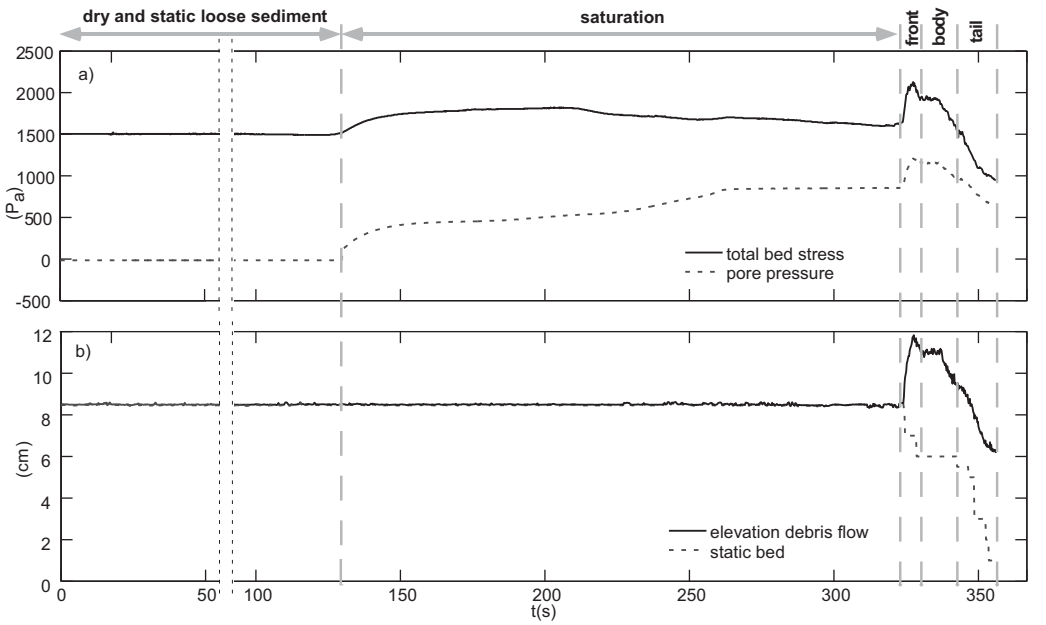

Figure 3. Data acquired 0.5 m from the end section of the downstream tributary flume (C) during run 14 (tributary slope of 17°, confluence angle 90°; simultaneous triggering): (a) total bed normal stress and pore fluid pressure measured at the rigid bed of the flume, thus including the contribution of the static sediment bed and of the overlaying debris flow; (b) free-surface elevation of the sediment-water mixture and elevation of the interface with the underlying static sediment bed.

to that documented by *Ancey* [2013] in the presence of a rigid bed, and by *Lanzoni and Tubino* [1993] for an underlying static bed made of loose sediment. However, in the presence of a loose sediment bed the flow depth is characterized by two well defined superposed layers. The dynamics of the upper layer is dominated by grain collisions while the lower, much slender layer is controlled by quasi-static forces due to enduring contacts between grains. It must be also stressed that, at the end of a given experiment, the elevation of the sediment surface measured just before a confluence with the main channel can attain a value either smaller (indicating an overall erosion) or larger (overall deposition) than the initial static bed surface, depending on the tributary slope and the geometry of the sediment deposits in the main channel. Generally, lower slopes and larger confluence angles favor deposition.

A clearer description of the various debris flow propagation stages is attained by eliminating from the signals recorded by the load cell and the pressure transducer the contribution due to the static portion of the gravel bed, assumed to be characterized by a hydrostatic distribution of the pore fluid pressure (see section 2.3). This speculation is confirmed by the measurement provided by the pore fluid pressure transducer. Figure 4 shows the temporal distribution of the piezometric head, $\sigma_{fb}/(\rho_f g)$, measured at the rigid bed of the flume during test 14, and that resulting by assuming a hydrostatic distribution (i.e., $\rho_f g H \cos\beta$). The deviations from an hydrostatic distribution are quite small, lower than 0.5 cm. Note that, just before the arrival of the front, the piezometric head is practically equal to the thickness of the saturated bed, the error being of the same order of the sediment grain size. In summary, no significant excess pore fluid pressure occur in the present tests. Such result agrees with the experimental findings of *Hotta* [2012], who carried out debris flow experiments with a similar sediment (mean grain size 2.9 mm) and the same slope (17°).

The temporal evolution of the relevant variables observed in run 14 and described in Figure 3 can be better appreciated by describing the passage of the debris flow at a given section in terms of the total basal normal stress, σ_b, the flow depth D, the bulk density, ρ (scaled by its maximum value, ρ_{max}), and the bulk concentration of the sediment-water mixture, C. The enlarged view of the time series of these quantities, reported in Figure 5, emphasizes that flow depth and basal normal stress, as well as high mixture density and sediment concentration increase at the front, keep nearly constant during the passage of the body, and decrease progressively during the passage of the tail. This behavior is quite similar to that observed in the laboratory by *Hotta* [2012] and in the Acquabona Watershed (Italian Alps) by *Berti et al.* [2000]. Moreover, the increase of σ_b

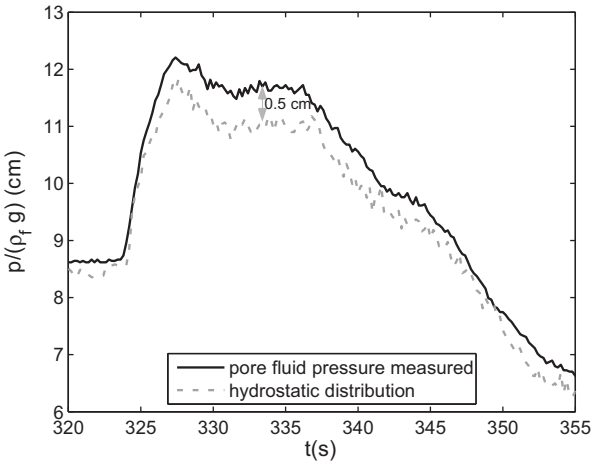

Figure 4. Temporal evolution of the pore fluid pressure, scaled by $g\,\rho_f$ (piezometric head), measured 0.5 m from the end of the downstream tributary (flume C) (run 14: tributary slope 17°; confluence angle 90°; simultaneous triggering). The piezometric head measured at the rigid flume bed through the pressure transducer is compared with the hydrostatic pressure $\rho_f\,g\,H\cos\beta$, resulting by considering the free-surface elevation H of the sediment-water mixture surface, referred to the rigid flume bed, recorded by the acoustic level sensor.

proportionally to D is in accordance with the observations of *Major and Iverson* [1999]. Here a maximum value of $\sigma_b \sim$ 900 Pa is observed during the passage of the debris front (lasting about 5 s), with an associated flow depth of ∼5 cm. The transit of the debris flow body lasts about 8 s (between 329 and 337 s) and is associated with an almost steady condition ($D = 5$ cm; $\sigma_b = 800$ Pa). Finally, both σ_b and D experience a slow and gradual reduction due to the passage of the long debris flow tail. On the other hand, the bulk density of the mixture attains a maximum at the debris flow front, decreases slightly until it stabilizes around the value ∼1700 kg/m^3, during the passage of the body, and decreases slowly in the debris tail. A similar behavior is exhibited by the mixture concentration C, which attains a value of ∼0.43 in the debris flow body.

The overall behavior of the water-sediment mixture emerging from the temporal series of the monitored quantities (Figure 5) is independent of the tributary slope, at least for the range of parameters examined in the present series of tests. In general, decreasing the tributary slope implies smaller bulk mixture density and sediment concentration, in accordance with the experimental findings of *Armanini et al*. [2005] for mature debris flows conditions. For a tributary slope of 15° (Figure 6) the sediment concentration of the body takes an average value ∼0.3. In addition, the front tends to elongate (longer duration) and the body becomes more irregular. The longer duration is due to the larger time that, for a lower bulk concentration, it takes to erode the fixed volume of sediment initially placed in the flume. On the other hand, the irregularities experienced by the body are strictly related to oscillations in the vertical structure of the flow, documented by the sidewall images acquired during the experiments. In the case of lower slopes the entrainment process appears to be more intermittent and implies a fluctuation of the thickness of the upper and lower layers characterizing the flow, dominated by grain collisions and frictional long lasting contacts, respectively.

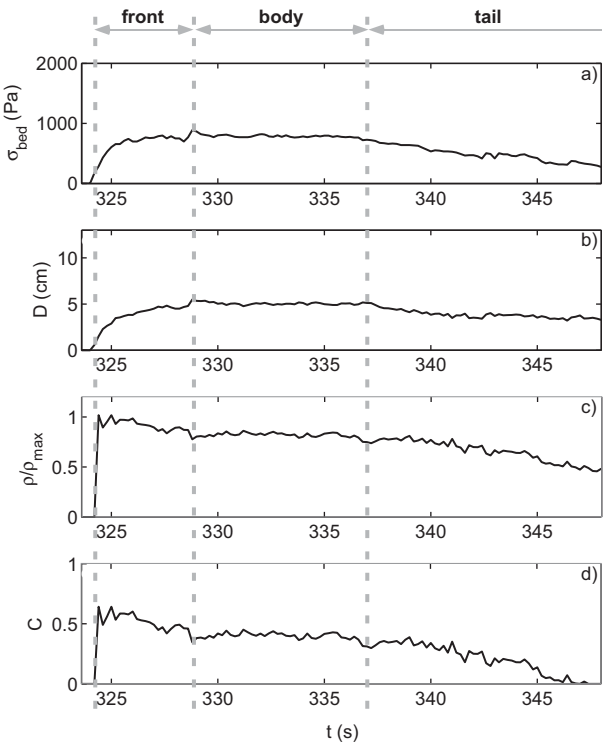

Figure 5. Temporal distribution of (a) total bed normal stress (Pa); (b) debris flow depth (cm); (c) density of the sediment-water mixture, scaled by its maximum value; (d) bulk sediment concentration of the debris flow mixture. All measurements have been carried out 0.5 m from the end of the downstream tributary flume during run 14 (tributary slope 17°; confluence angle 90°; simultaneous triggering).

3.2. Deposit Geometry

The present experiments provide useful information also on the morphology of sediment deposits formed in the main

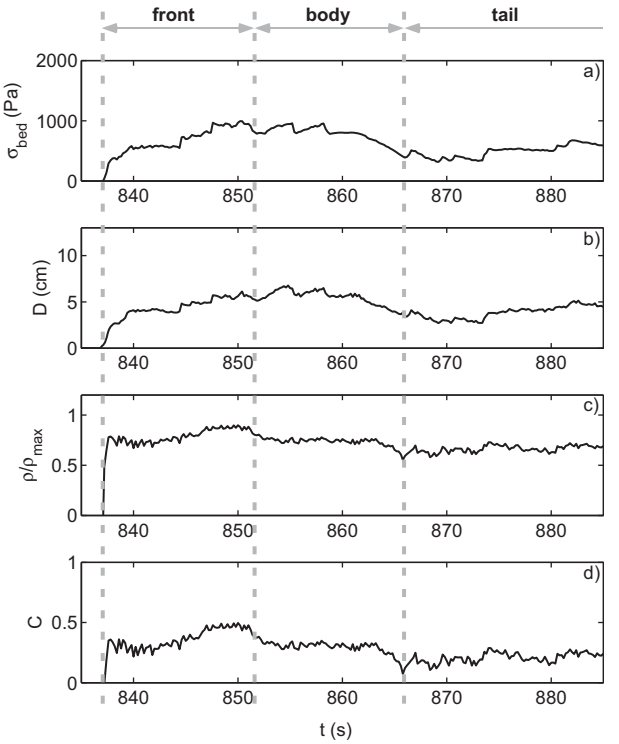

Figure 6. Temporal distribution of (a) total bed normal stress (Pa); (b) debris flow depth (cm); (c) density of the sediment-water mixture, scaled by its maximum value; (d) bulk sediment concentration of the debris flow mixture. All measurements have been carried out 0.5 m from the end of the downstream tributary flume during run 13 (tributary slope 15°; confluence angle 90°; simultaneous triggering), characterized by tributary slope angle of 15°.

channel by debris flows generated in lateral tributaries. The form and duration of the sediment pulses within the main channel are determined by the interplay of bulk concentration and velocity of the water-sediment mixture in the tributaries. As described above, the concentration of this mixture tends to increase with the tributary slope. Higher concentrations, in turn, tend to decrease debris flow mobility (i.e., the bulk flow velocity). The tributary slope is thus a parameter that crucially affects the geometry of sediment deposits. Further quantities that likely play a nonnegligible role are the confluence angle and the triggering sequence of inflowing debris waves. Note that, even though the volume of sediment that can be mobilized is always the same, the form of the debris hydrograph and the duration of the phenomenon influences the amount of sediment that can be removed by the main channel flow and, hence, the overall volume that deposits in the main channel at the end of a given test.

The most dangerous configuration is associated with the highest value of the tributary slope (17°) and with a simultaneous triggering. Figure 7 summarizes, for the entire set of data, the results of the analysis carried out on sediment deposit geometry on the basis of the bed topography eventually surveyed along a few longitudinal main channel sections (see Figure 2). The investigated parameters are the sediment deposit volume V_s, the position of its center of mass (x_G,y_G, z_G), and the standard deviations, σ_x and σ_y, of the sediment surface elevation for the entire deposit forming in the main channel (see Figure 1 for the definition of the axes x and y along which σ_x and σ_y are computed). On average, V_s tends to increase with the tributary slope and the confluence angle. The center of mass is always located downstream of the axis of symmetry of the two confluences (x= 210 cm), owing to the sediment transport caused by the main channel flow. In general, the larger channel obstruction (smaller Y_G) occurs for simultaneous triggering and the larger confluence angles, although some scatter appears. No significant trend is noticed for the vertical position of the center of mass.

The specific shapes of the two deposit fans formed in the main channel, in the case of simultaneous triggering, are analyzed in Figure 8. Each deposit is schematized with an ellipse localized at its center of mass (x_G, y_G) and with the two axes given by the standard deviations σ_x and σ_y of bed elevation now computed for every deposit. The experiment with higher tributary slope (run 14) exhibits the larger transverse dimension of the ellipses and, hence, a greater degree of obstruction; moreover, the centers of mass of the two fans are slightly closer. On the other hand, increasing the confluence angle (runs 12, 9, and 13) results in an upstream shift of the deposit location and in a larger obstruction at the second confluence.

A schematic overview of the geometry of the sediment deposits and their interaction as confluence angle, triggering scenario and tributary slope change is displayed in Figure 9. The sketches clearly show: the upstream migration of the centers of mass as the confluence angle increases; the increase of main channel obstruction when debris waves are triggered simultaneously in the two tributaries and for higher tributary slopes. As previously noted, the volume of debris that enters the main channel is strongly

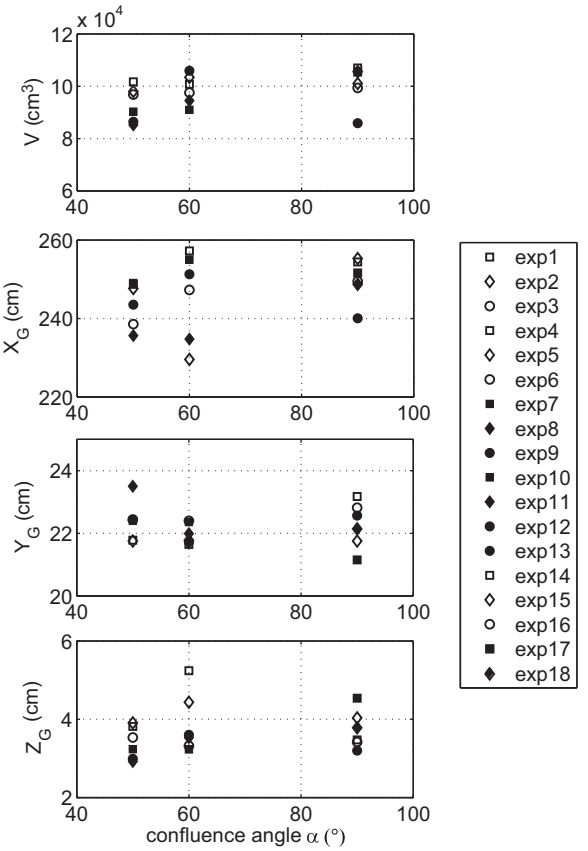

Figure 7. The overall volume, V_s, and the coordinates x_G, y_G, z_G of the center of mass of the sediment deposits are plotted versus the confluence angle for the entire experimental data set. Here x, y, and z are the longitudinal, transverse, and vertical (pointing upward) coordinates depicted in Figure 1. Full and empty symbols denote tributary slopes of 15° and 17°, respectively. Circles denote simultaneous triggering ($B = C$); squares represent debris flow occurring first in the upstream tributary ($B < C$), while diamonds denote debris flow occurring first in the downstream tributary ($B > C$).

controlled by the bulk density of the water-sediment mixture and the duration of the flow (i.e., the debris flow mean velocity). High degrees of river obstruction are associated with large enough values of density and duration. Low debris concentration favors the removal by the main river flow of the deposited sediment. Conversely, high debris concentration tends to decrease debris flow mobility. Hence, the propagation in the tributary channel and the deposition in the main channel take a longer time, with a consequent longer duration of the reworking action exerted on sediment deposit by the main channel flow.

Information on the vertical structure of the sediment deposits is provided in Figure 10, displaying the longitudinal bed profiles acquired along the centerline of the main channel in different tests. In order to quantify the degree of mutual interaction between the two deposits we introduce the interference h_{in}, defined as the maximum thickness of the sediment deposit that marks the transition between the upstream and the downstream debris fans. Figure 10a reports a general comparison for all the experiments carried out with a tributary slope of 17°, the same triggering scenario (downstream-upstream triggering sequence), but varying the confluence angle ($\alpha = 50°$-$60°$-$90°$). The larger value of h_{in} (7.3 cm), and hence the stronger degree of obstruction of the main channel, is observed for $\alpha = 90°$. Figure 10b shows the longitudinal bed profiles measured at the end of three runs characterized by the same tributary slope (17°), the same confluence angle (90°), and different triggering scenarios. The first scenario ($t_B < t_C$, upstream-downstream triggering) implied a relatively small value of h_{in} (=4.5 cm), located toward the downstream confluence and near the main flume bank hosting the tributary outlets. The second scenario ($t_B > t_C$, downstream-upstream triggering) was characterized by a slight upstream shift and a growth of h_{in} (=7.3 cm). Finally, in the third scenario ($t_B = t_C$, simultaneous triggering) h_{in} (=8.9 cm) further increases and its position tends to move away from the bank hosting the confluences, thus leading to a greater obstruction of the hydraulic section of the main channel. In general, a larger deposit interference is observed for a simultaneous triggering $t_B = t_C$, while a medium interference occurs for the downstream-upstream triggering sequence $t_B > t_C$. Almost no interference occurred for the upstream-downstream triggering sequence. Figure 10c indicates that higher deposit interference ($h_{in} =$ 8.9 cm) is attained, as expected, for a higher tributary slope (17°) and a simultaneous triggering of the debris waves.

4. Discussion

Natural debris flows are usually characterized by a stress regime intermediate between inertial and frictional, or tend to be friction dominated if fine fractions are relatively abundant in the sediment composition. In this latter case, in fact, sediment concentration can approach or exceed the threshold (~0.5)

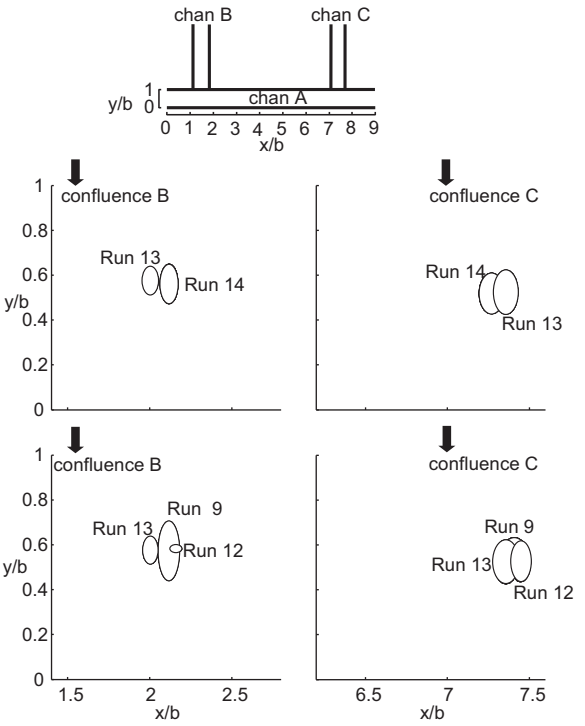

Figure 8. Shape analysis of the deposit formed in the main channel by each tributary, surveyed at the end of runs 13 and 14, characterized by different tributary slopes, and at the end of runs 9, 12, and 13, characterized by different confluence angles (see Table 1). Each ellipse is localized in the center of mass of each deposit and its principal axes are given by the standard deviations of the sediment surface elevation of each deposit along the *x* and *y* directions.

for which Coulomb friction stresses predominate [*Campbell*, 1990; *Takahashi*, 2007]. Coarse sediment, on the other hand, favors the establishment of the inertial regime. A spatially varying stress regime can also develop within a given debris flow, depending on the different sediment composition of the front (coarser), body and tail (finer) [*Campbell*, 2002, 2005]. The present experiments, intended to address stony debris flow behavior and, hence, have been carried out by using a nearly uniform gravel material. Indeed, stony-type flows usually exhibit a relatively low content of fines, mainly included in the interstitial muddy water which behaves as a liquid, as well as small depth to mean grain size ratio (less than about 20–30) and, consequently, not too high bulk solid concentration (0.35–0.62 by volume) [*Bonnet-Staub*, 1999; *Takahashi*, 2007]. In natural environment this type of phenomena can be generated on scree slopes and in high slope torrents. Clearly, the presence of fine material in the mixture can influence both debris flow triggering [*Chen et al*., 2010] and propagation [*Sosio and Crosta*, 2009; *Kaitna et al*., 2014]. When solid fractions less than 0.1 mm is 10–30%

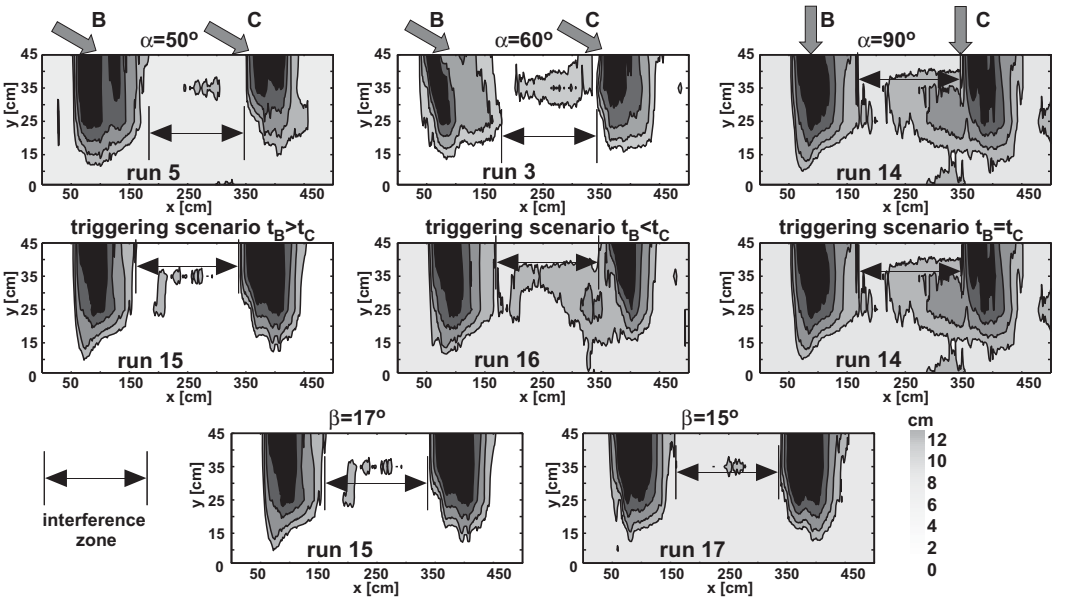

Figure 9. Overall view of the deposits surveyed along the main channel at the end of tests carried by varying the (top) confluence angle (tributary slope 17°; simultaneous triggering), (middle) triggering scenario (tributary slope 17°; confluence angle 90°), and (bottom) tributary slope (confluence angle 90°; upstream-down triggering sequence).

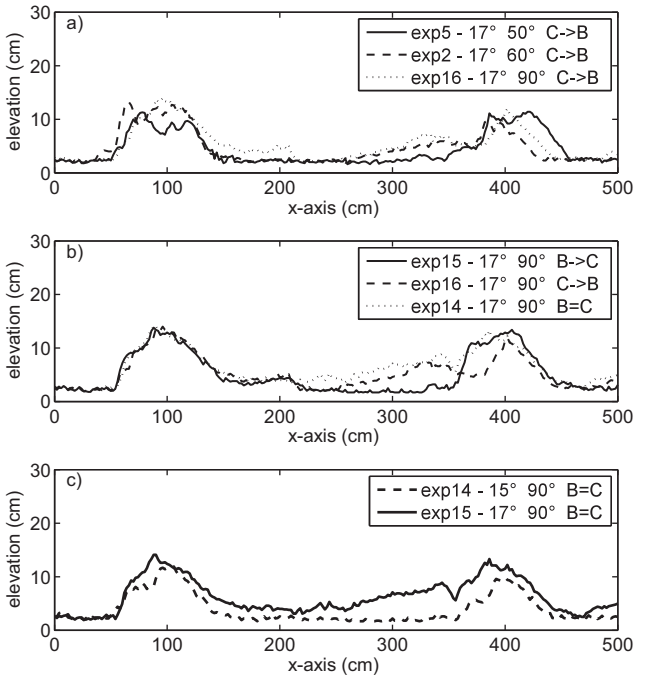

Figure 10. Mutual interaction between the deposits generated in the main channel nearby the two confluences, in terms of interference (i.e., maximum thickness of the sediment deposit that marks the transition between the upstream and the downstream debris fans). Longitudinal bed profiles have been measured along the centerline of the main channel at the end of experiments carried out with (a) fixed slope (17°) and triggering scenario (downstream-upstream triggering sequence), but variable confluence angles (50°–60°–90°); (b) fixed slope (17°) and confluence angle (90°), but different triggering scenarios (upstream-downstream triggering sequence; downstream-upstream triggering sequence; simultaneous triggering); (c) same confluence angle (90°) and triggering condition (simultaneous triggering), but different tributary slopes (15°–17°).

of the sediment mixture composition, turbulent muddy-type debris flows or viscous-type debris flows occur. The solid concentration takes larger values (0.45–0.75) and, owing to the smaller value of the representative grain size, the relative flow depth (i.e., scaled with the mean sediment diameter) attains values much larger than 20–30. Sediment mobility increases significantly with the content of fines: stony-type debris flows have larger resistance to flow than muddy-type flows, which, in turn, has a slightly smaller mobility than muddy debris flows and plain water flows [*Takahashi*, 2007]. Finally, the presence of silt and clay material, promotes the persistence of high pore pressures [*Iverson et al*., 2010].

Analysis presented in section 2.4 indicates a prevailing collision-dominated regime, typical of mature stony debris flows. Nevertheless, even though the observed bulk concentration was always smaller that the threshold value (0.5) discriminating a friction dominated behavior, the presence of a loose static bed determines the formation of a lower layer in which the long-lasting contacts between particles generate non negligible quasi-static stresses. This is confirmed by the sidewall images collected during the tests and, indirectly, by the estimates of the bulk concentrations. For example, the value observed in run 14 ($\sim$0.43) is larger than that (0.30) obtained by means of the empirical formula developed by *Takahashi* [2007]:

$$c_s = \frac{\rho_f \tan\beta}{(\rho_s - \rho_f)(\tan\varphi - \tan\beta)}. \quad (6)$$

This relation has been determined for stony debris flows propagating over a rigid bed and, hence, with a minor effects of quasi-static actions near the bed. In order to obtain a correct estimate of the bulk concentration, the long lasting grain interactions at the boundary between the upper, grain inertial layer and the underlying static sediment bed should be accounted for. This is done by replacing into equation (6) the static friction angle of the sediment ($\varphi = 43.3°$) with a smaller value ($\sim$36.5° for the present material) [*Lanzoni and Tubino*, 1993; *Egashira et al*., 1997; *Iverson*, 1997].

The tests considered so far have been conducted by using almost the same amount of water to trigger debris flows in the tributaries and keeping fixed the water discharge in the main channel. Considering that the tests summarized in Table 1 are already affected by variations of the triggering discharge of the order of a 10% with respect to the mean value adopted in the experiments, we have performed two additional tests by saturating the tributary flumes with a seepage discharge of 0.8 l/s and triggering the sediment-water flow with a water discharge of either 3 or 2.7 l/s. A tributary slope of 17° and a confluence angle of 90° have been considered, while the discharge in the main channel has been set to zero for facilitating the comparison. Figure 11 shows three different longitudinal profiles and a transverse profile surveyed at the end of these two additional tests: minor differences are observed both in terms

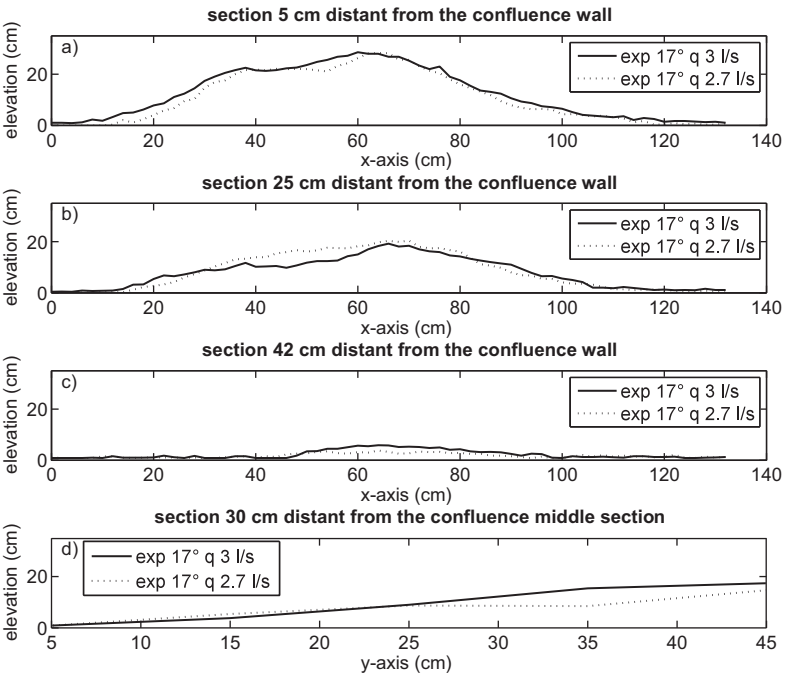

Figure 11. Comparison between profiles of the deposit acquired for a tributary slope of 17° and triggering water discharges of 3 l/s (solid line) and 2.7 l/s (dashed line). Longitudinal profiles surveyed at a distance of (a) 5 cm, (b) 25 cm, and (c) 42 cm from the main channel bank hosting the confluences. (d) Transverse profile measured in a section located 30 cm downstream of the intermediate section between confluences.

of planar displacement and deposit height. Therefore, relatively small differences of the water discharge used to trigger the debris flows in a tributary are likely to induce only small variations in the concentration and propagation speed of the sediment-water mixture, which are mainly controlled by the tributary slope.

The role of the main channel flow in shaping the debris deposits also merits a brief discussion. For values of the water discharge Q_A much larger than the sediment-water flux conveyed by tributaries, the sediment deposits tend to be rapidly washed out. Conversely, when the intensity of the main channel flow is low as compared to the injected debris flow, a backward deposition can take place in the tributary, favoring the main channel obstruction [*Chen and An*, 2007]. In general, the complete blockage is controlled by the velocity ratio and discharge ratio between the tributary and the mainstream, as well as by the confluence angle and the degree of sediment sorting [*Dang et al.*, 2009]. In the case of almost homogeneous sediments, these parameters can be combined to form a single dimensionless parameter, the momentum ratio, $R_M = R_Q R_u R_\rho \sin\beta$, where R_Q is the discharge ratio; R_u, is the velocity ratio; R_ρ is the bulk density ratio, defining the relative importance of a given quantity in the tributary and in the mainstream [*Dang et al.*, 2009]. A complete obstruction of the main channel requires high enough values of both the discharge ratio and the velocity ratio (greater than 3.37 and 1.1,

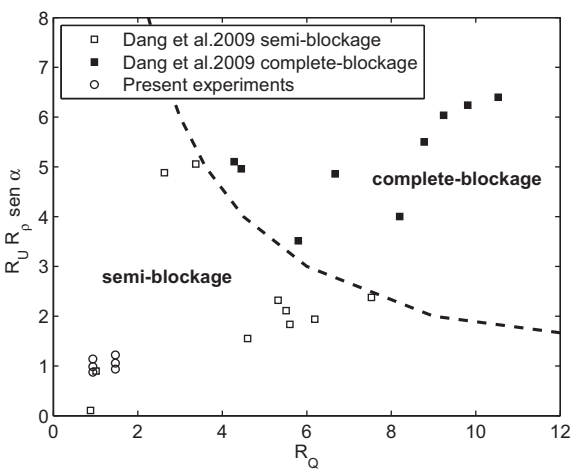

Figure 12. Threshold of complete-partial main channel obstruction (dashed line), identified with data of the present experiments and that of *Dang et al.* [2009].

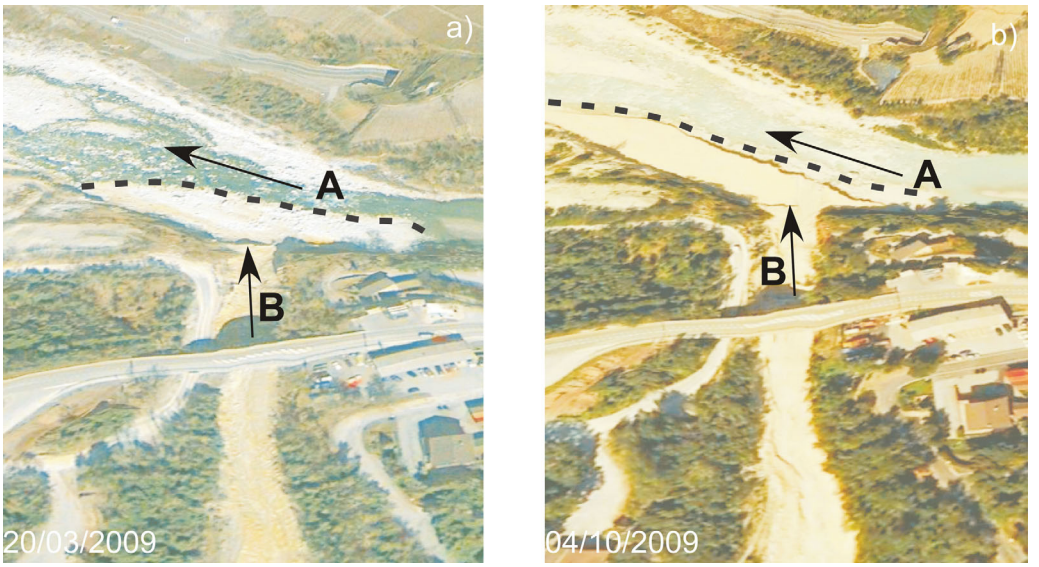

Figure 13. Views of the confluence of the torrent Illgraben (B) with the Rhone river (A) before (20 March 2009) and after (4 October 2009) a debris flow event. The images have been taken form Google Earth (46°18′N, 7°38′E). The alluvial fan (dashed line) formed in the main channel (A) after a debris flow event in the tributary (B) just forces the water flow to the opposing river bank. In particular, plate (b) shows that a significant amount of deposited sediment is not yet completely removed and transported downstream by the main channel water flow.

respectively, according to *Dang et al.*'s [2009] laboratory experiments); conversely, small values of these ratios favor the washing out of the debris conveyed by tributaries. Main channel obstruction is also enhanced by larger bulk densities (and, hence, higher tributary slopes) and greater degree of sediment gradation. Figure 12 compares the present data with those obtained from the experiments carried out by *Dang et al.* [2009]. In addition, the figure shows the line $R_M = 18$, defining the critical threshold discriminating between partial and complete blockage. The plot indicates that in the present set of experiments a condition of semiblockage is invariably attained: the debris flow, in fact, never reached the main channel bank opposite to the confluence. In other words, the deposit fan forces the main channel to contour it, narrowing the active section throughout which the water flows. A situation in which the alluvial fan does not block the main channel, but just forces it to the opposing river bank, shrinking the areas available for water flow (e.g., the Illgraben fan on the upper Rhone in Valais, Figure 13).

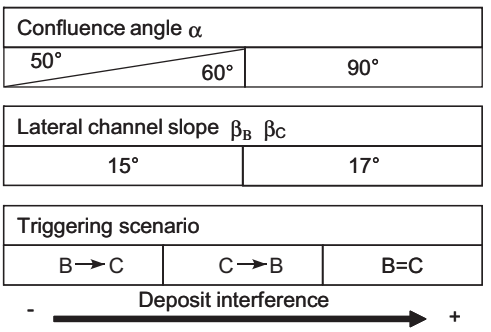

Figure 14. Synopsis of the information obtained from the analysis of the present experimental data, showing that greater interference (defined as the maximum thickness of the sediment deposit in the main channel that marks the transition between the upstream and the downstream debris fans) is caused by greater confluence angle, greater slope of adjacent tributary channels (B and C), and simultaneous triggering of debris flows within them.

5. Conclusion

The dynamics of stony debris flows formed in two adjacent tributaries and depositing into the same channel has been investigated experimentally. This schematic configuration intended to reproduce the intense and rapid gravity-driven movements of water and gravel generated on the scree slopes at the base of rock faces. This material, as often observed in the Dolomites (Northern Italy) is subsequently delivered in a main, less sloping channel through relatively close confluences.

1. The sediment-water flows generated in the present tests formed in the upstream portion of a tributary and then propagated downstream, with almost negligible erosion of the underling static bed, until the arrival of the debris flow tail. As a consequence, at a given gauging section, three different phases were observed, corresponding to the passage of the front,

the body and the tail of the debris flow. The values of the relevant dimensionless parameters (Bagnold, Savage and Mass numbers) estimated for the present tests suggest an overall prevalence of internal stresses generated by grain collision, as typically occur in stony debris flows. In addition, the analysis of the temporal sequences of total normal stress, pore fluid pressure and elevation of the sediment-water mixture surface indicates a negligible contribution of the excess pore fluid pressure. The bulk (depth averaged) concentration within the debris flow body, estimated on the basis of the total normal stress at the interface with the static bed and the flow depth, indicates that the concentration increases with the tributary slope. Its value is under-predicted by the relation proposed by *Takahashi* [2007]. A more reliable estimate requires that a quasi-static friction angle, instead of the submerged static friction angle, is employed in this relation. In the presence of a debris flow propagating over a loose sediment bed, in fact, the quasi-static actions induced by long-lasting grain contacts play some role in determining the overall debris flow dynamics also when a grain collision regime prevails in most of the mixture column. Moreover, the rate of sediment entrainment that takes place in the lower slender layer of the flow where quasi static stresses prevail, depends on the tributary slope rather than on the water flow discharge used to trigger the debris flow.

2. The morphological analysis of the debris deposits settled on the bed of the receiving channel suggests that the sediments delivered by the tributaries tend to be washed out for low confluence angle (50°) and low tributary slopes (15°). Conversely, the thickness of sediment deposits tends to increase for a perpendicular confluence and higher tributary slopes (17°), enhancing both the interference between the deposits at adjacent confluences and the probability of channel damming. In addition, increasing the tributary slope and the confluence angle produces a faster debris flow propagation and, hence, further limits the time available for warning.
3. The most dangerous scenario, yielding the higher degree of obstruction in the receiving channel, is obtained when debris flows are triggered simultaneously in the tributary channels, no matter which confluence angle and tributary slope have been considered. A relatively dangerous scenario is also observed when the debris flows are triggered firstly downstream and then upstream.
4. The present data set, collected under highly controlled experimental conditions, provides a unique opportunity for calibration, validation and further improvement of mathematical models of debris flow generation, propagation, and settlement.

In summary, the risk of significant obstruction in a river reach as a consequence of the lateral injections of similar volumes of sediments delivered by multiple debris flows tends to increase with the tributary slope angle and the confluence angle, and tends to be maximum if debris flows take place simultaneously (Figure 14).

Clearly, other factors, not considered here, can influence the process. Although none are likely to modify the gross features of the phenomenon emerged from the present analysis, they merit to be studied in the near future. The water flow in the main channel, whose features are strictly related to the bed slope, surely has an important role in determining the shape of the debris fans and in removing the debris deposits. The effects of a nonnegligible content of fine (silty and clay) material in the fluid used to mobilize the debris flows certainly also need to be investigated. In particular, it is of interest to quantify the percentage of fines above which the pore fluid pressure does not dissipate and, hence, plays a certain role in controlling the dynamics of the propagation phase, as well as dewatering and consolidation of the sediment deposits. Finally, it should be studied how the mutual interference between adjacent deposits varies with the distance between the confluences.

Acknowledgments
This work was supported by the project GAPDEMM "GIS-based integrated platform for Debris Flow Monitoring, Modeling and Hazard Mitigation," funded by CARIPARO foundation. These results are part of the PhD thesis of L.M.S. partly supported by the University of Catania and University of Padova. All the data concerning this paper (temporal series used to draw the various plots, results of the analysis carried out on the sediment deposit geometry, raw videos) are available by contacting the corresponding author.

References

Ancey, C. (2013), *Gravity Flow on Steep Slope, in Buoyancy-Driven Flows*, edited by E. P. Chassignet, C. Cenedese, and F. Verron, pp. 372–432, Cambridge Univ. Press., N. Y.
Armanini, A., H. Capart, L. Fraccarollo, and M. Larcher (2005), Rheological stratification in experimental free-surface flows of granular-liquid mixture, *J. Fluid Mech.*, *532*, 269–319.
Benda, L. (1990), The influence of debris flows on channels and valley floors in the Oregon Coast Range, U.S.A., *Earth Surf. Processes Landforms*, *15*, 457–466.
Berti, M., R. Genevois, A. Simoni, and P. R. Tecca (1999), Field observations of a debris flow event in the Dolomites, *Geomorphology*, *29*, 256–274.
Berti, M., R. Genevois, R. LaHusen, A. Simoni, and P. R. Tecca (2000), Debris flow monitoring in the acquabona watershed on the Dolomites (Italian alps), *Phys. Chem. Earth, Part B*, *25*(9), 707–715.
Bonnet-Staub, I. (1999), Definition d'une typologie des deposits de laves torrentielles et identification de critres granulomtriques et geotechniques concernant les zones sources, *J. Bull. Eng. Geol. Environ.*, *57*(4), 359–367.
Campbell, C. S. (1990), Rapid granular flows, *Annu. Rev. Fluid Mech.*, *22*, 57–92.
Campbell, C. S. (2002), Granular shear flows at the elastic limit, *J. Fluid Mech.*, *465*, 261–291.
Campbell, C. S. (2005), Stress-controlled elastic granular shear flows, *J. Fluid Mech.*, *539*, 273–297.

Chen, N. Sh., W. Zhou, Ch. L. Yang, G. Sh. Hu, Y. Ch. Gao, and D. Han (2010), The processes and mechanism of failure and debris flow initiation for gravel soil with different clay content, *Geomorphology*, *121*, 222–230.
Chen, R. D., X. N. Liu, S. Y. Cao, and Z. X. Guo (2011), Numerical simulation of deposit in confluence zone of debris flow and mainstream, *Sci. China Technol. Sci.*, *54*(10), 2618–2628.
Chen, R. D., X.-N. Liu, E. Huang, and Z.-X. Guo (2013), Numerical analysis of emergency river restoration scheme for Qingping mega debris flow, *J. Mountain Sci.*, *10*(1), 130–136.
Chen, S. C., and S. An (2007), Flume experiment of debris flow confluence formed alluvial fan in the main channel, in *River, Coastal and Estuarine Morphodynamics: RCEM 2007*, edited by C. M. Dohmen-Janssen and S. J. M. H. Hulscher, pp. 829–835, Taylor and Francis, London, U. K.
Chen, S. C., S. H. Peng, and H. Capart (2004), Morphology of alluvial fans formed by hyperconcentrated tributaries, in *Proceedings of the 2nd International Conference on Fluvial Hydraulics, Napoli, Italy*, edited by M. Greco, A. Carravetta, and R. Della Morte, pp. 1095–1102, Taylor and Francis Group, London, U. K.
Chen, S. C., and S. H. Peng (2006), Two-dimensional numerical model of two-layer shallow water equations for confluence simulation, *Adv. Water Resour.*, *29*(11), 1608–1617.
Dang, C., P. Cui, and Z. I. Cheng (2009), The formation and failure of debris flow-dams, background, key factors and model tests: Case studies from China, *Environ. Geol.*, *57*, 1901–1910.
Davies, T. R. H. (1990), Debris-flow surges: Experimental simulation, *J. Geol. N. Z.*, *29*(1), 18–46.
Denlinger, R. P., and R. M. Iverson (2001), Flow of variably fluidized granular masses across three-dimensional terrain: 2. Numerical predictions and experimental tests, *J. Geophys. Res.*, *106*, 553–566.
Egashira, S., K. Miyamoto, and T. Itoh (1997), Constitutive equations of debris flow and their applicability, in *Proceedings of the 1st International Conference on Debris-Flow Hazards Mitigation*, edited by C.-L. Chen, pp. 340–349, Am. Soc. of Civ. Eng., N. Y.
Gregoretti, C. (2000), The initiation of debris flow at high slopes: Experimental results, *J. Hydraul. Res.*, *38*, 83–88.
Gregoretti, C., and G. Dalla Fontana (2008), The triggering of debris flows due to channel-bed failure in some alpine headwater basins of Dolomites: Analyses of critical runoff, *Hydrol. Processes*, *22*, 2248–2263.
Heller, V. (2011), Scale effects in physical hydraulic engineering models, *J. Hydraul. Res.*, *49*, 293–306.
Hoblitt, R. P. (1986), Observations of the eruptions of July 22 and August 7, 1980, at Mount St. Helens, Washington, *U.S. Geol. Surv. Prof. Pap.*, *1335*, 44.
Hotta, N. (2012), Basal interstitial water pressure in laboratory debris flows over a rigid bed in an open channel, *Nat. Hazards Earth Syst. Sci.*, *12*, 2499–2505.
Hsu, K. J. (1975), Catastrophic debris streams (sturzstroms) generated by rockfalls, *Geol. Soc. Am. Bull.*, *86*, 129–140.
Hsu, K. J. (1978), Albert Hiem: Observations on landslides and relevance to modern interpretations, in *Rockslides and Avalanches: Natural Phenomena*, edited by B. Voight, vol. 1, pp. 71–93, Elsevier, Amsterdam, Netherlands.
Hsu, L., W. E. Dietrich, and L. S. Sklar (2008), Experimental study of bedrock erosion by granular flows, *J. Geophys. Res.*, *113*, F02001, doi: 10.1029/2007JF000778.
Iverson, R. M. (1997), The physics of debris flows, *Rev. Geophys.*, *35*, 245–296.
Iverson, R. M. (2013), Mechanics of debris flows and rock avalanches, in *Handbook of Environmental Fluid Dynamics*, edited by H. J. S. Fernando, vol. 1, pp. 573–587, CRC Press, Boca Raton, Fla.
Iverson, R. M., and R. P. Denlinger (2001), Flow of variably fluidized granular masses across three-dimensional terrain: 1. Coulomb mixture theory, *J. Geophys. Res.*, *106*, 537–552.
Iverson, R. M., and J. W. Vallance (2001), New views of granular mass flows, *Geology*, *29*(2), 115–118.
Iverson, R. M., M. Logan, R. G. LaHusen, and M. Berti (2010), The perfect debris flow? Aggregated results from 28 large-scale experiments, *J. Geophys. Res.*, *115*, F03005, doi:10.1029/2009JF001514.
Kailey, P., E. T. Bowman, J. Laue, and S. M. Springman (2011), Modelling debris flow processes with a geotechnical centrifuge, *Ital. J. Eng. Geol. Environ.*, *3*, 339–349.
Kaitna, R., W. E. Dietrich, and L. Hsu (2014), Surface slopes, velocity profiles and fluid pressure in coarse-grained debris flows saturated with water and mud, *J. Fluid Mech.*, *7*, 377–403.
Kuntz, M. A., P. D. Rowley, N. S. MacLeod, R. L. Reynolds, L. A. McBroome, A. M. Kaplan, and D. J. Lidke (1981), Petrography and particle size distribution of pyroclastic-flow, ashcloud, and surge deposits, *U.S. Geol. Surv. Prof. Pap.*, *1250*, 525–539.
Lanzoni, S., and M. Tubino (1993), Rheometric experiments on mature debris flows, in *Proceedings of XXV International Association for Hydro-Environment Engineering and Research Congress*, pp. 47–54, IAHR, Tokyo.
Major, J. J., and R. M. Iverson (1999), Debris-flow deposition effects of pore-fluid pressure and friction concentrated at flow margins, *Geol. Soc. Am. Bull.*, *111*, 1424–1434.
Millard, T. (1999), Debris flow initiation in coastal British Columbia Gullies, *For. Res. Tech. Rep. TR-002*, Vancouver For. Reg., B. C. For. Serv., Nanaimo, B. C., Canada. [Available at https://www.for.gov.bc.ca/rco/research/georeports\tr002.pdf.]
Miller, D. J., and K. M. Burnett (2008), A probabilistic model of debris-flow delivery to stream channels, demonstrated for the Coast Range of Oregon, USA, *Geomorphology*, *94*, 184–205.
Scheidl, C., and D. Rickenmann (2009), Empirical prediction of debris-flow mobility and deposition on fans, *Earth Surf. Processes Landforms*, *35*, 157–173.
Sharp, R. P., and L. H. Nobles (1953), Mudflow of 1941 at Wright-wood, southern California, *Bull. Geol. Soc. Am.*, *64*, 547–560.
Sitar, N., S. A. Anderson, and K. A. Johnson (1992), Conditions for initiation of rainfall-induced debris flows, in *Stability and Performance of Slopes and Embankments II*, pp. 834–849, Geotech. Eng. Div., Am. Soc. of Civ. Eng., N. Y.
Sklar, L. S., W. E. Dietrich, E. Foufoula-Georgiou, B. Lashermes, and D. Bellugi (2006), Do gravel bed river size distributions record channel network structure?, *Water Resour. Res.*, *42*, W06D18, doi:10.1029/2006WR005035.
Sosio, R., and G. B. Crosta (2009), Rheology of concentrated granular suspensions and possible implications for debris flow modeling, *Water Resour. Res.*, *45*, W03412, doi:10.1029/2008WR006920.
Takahashi, T. (1991), *Debris Flow*, 165 pp., A. A. Balkema, Brookfield, Wis.
Takahashi, T. (2007), *Debris Flows: Mechanics, Prediction and Countermeasures, Proc. Monogr. Eng. Water Earth Sci.*, Taylor and Francis, Leiden.
Tognacca, C., G. R. Bezzola, and H. E. Minor (2000), Threshold criterion of debris-flow initiation due to channel bed failure, in *Proceedings of the Second International Conference on Debris Flow Hazards Mitigation*, edited by G. F. Wiezczorek and N. D. Naeser, pp. 89–97. A.A. Balkema Rotterdam.
Wilson, L., and J. W. Head (1981), Morphology and rheology of pyroclastic flows and their deposits, and guidelines for future observations, *U.S. Geol. Surv. Prof. Pap.*, *1250*, 513–524.